



## Novel, Low Cost and Fast Detection Sensor for Biogenic H<sub>2</sub>S Gas Based on Polyaniline/ZnO, CdO and CeO<sub>2</sub> nanocomposites at Room Temperature



CrossMark

Khalid I. Kabel<sup>1\*</sup>, A. Labena<sup>2</sup>, Walaa S. Gado<sup>3</sup>

<sup>1</sup> Petroleum Applications Department, Egyptian Petroleum Research Institute (EPRI), Nasr City 11727, Cairo, Egypt.

<sup>2</sup> processes design and development Department, Egyptian Petroleum Research Institute (EPRI), Nasr City 11727, Cairo, Egypt.

<sup>3</sup> petrochemicals Department, Egyptian Petroleum Research Institute (EPRI), Nasr City 11727, Cairo, Egypt.

### Abstract

Screen printed electrode (SPE) is considering one of the most prospective techniques for sensing purposes due to its low cost, easy fabrication and reusability. It is worthwhile to use SPE as a sensor for fast detection of the biogenic H<sub>2</sub>S gas which is a sign for sulfate-reducing bacteria (SRB) existence. SRB presence is the first indicator in the industrial sector that causes a catastrophic environmental issue which give time for the decision makers to avoid their consequences. Polyaniline (PANI), PANI/MOx nanocomposites were prepared as sensing materials. The prepared materials have been characterized by FT-IR, Raman spectroscopy and GPC techniques. The morphological properties have been determined using SEM and HR-TEM. The particle size distributions have been determined using dynamic light scattering (DLS). Moreover, the fabricated sensors also have been applied as biogenic H<sub>2</sub>S gas detector using the electrical resistance changes. The data confirmed that the PANI doped with ZnO NPs has the best sensing performance compared to the other fabricated sensors.

*Keywords:* Sensors; Conducting polymers; Metal oxides; Nano-composites; H<sub>2</sub>S gas; and SRB.

### 1. Introduction

Sulphate-reducing bacteria (SRB) is anaerobic bacteria which can be exist in wastewater, soil and petroleum wells. The main problem of SRB is their metabolic process which reduce sulfate ions into sulfide ions. These sulfide ions can be present in a gas form as H<sub>2</sub>S gas or a dissolved form or a precipitated form (ferrous sulfide) [1-4]. Therefore, they have great economic and environmental impacts on the petroleum industry, due to corrosion severity and their toxic gases emission [4]. The corrosion problem of the pipelines and the production equipment's due to SRB metabolism, called biocorrosion or microbiologically influenced corrosion (MIC), which causes more than 20 % of the total corrosion cost [5-9]. Furthermore, SRB have the ability to make a biofilm, this phenomenon happens when the SRB contact with the iron surface especially at low stream flow and acting to mimic the surrounded conditions to protect themselves and hence causing more aggressive corrosion media in comparison to their planktonic counterparts. Biofilms can resist the biocide more than 1000 times comparing

to their planktonic forms [10]. The development of rapid and effective techniques for the SRB monitoring in natural and industrial environments have great efforts in last decades. The approaches employed to detect the presence of SRB are divided into two main categories: (i) culture-based and (ii) molecular-based methods [11,12]. Typically, the investigation of SRB using culture-based approach involves the isolation, cultivation and characterization of the bacteria using different growth media, such most probable number (MPN). For several decades the MPN has been widely used. The results take around 21 days for confirmation depending on the formation of ferrous sulfide black precipitate (FeS) [13]. Monitoring the H<sub>2</sub>S levels is very important for the oil and gas sector especially at lower concentrations. Nowadays, the industrial sector really in need of cheap, fast and highly sensitive detection techniques for H<sub>2</sub>S gas [14,15]. The electrochemical sensors are a low-cost solution for the monitoring the objective gas offering a valuable method with expanded scope, also high performance compared to the other traditional approaches [16-21].

\*Corresponding author e-mail: [drkhalid1977@yahoo.com](mailto:drkhalid1977@yahoo.com), [drkhalid1977@epri.sci.eg](mailto:drkhalid1977@epri.sci.eg); (Khalid I. Kabel).

Receive Date: 01 February 2021, Revise Date: 02 March 2021, Accept Date: 03 March 2021

DOI: 10.21608/EJCHEM.2021.60970.3308

©2021 National Information and Documentation Center (NIDOC)

The semiconductor-based electrodes and the metal oxide nanoparticles have been described for H<sub>2</sub>S gas sensing [22–26]. These metals are also assumed to have expanded catalytic activity on the electrochemical oxidation of sulfide gas. [27,28]. However, till now there are very restricted studies of utilize metallic based sensors such as nickel, gold and platinum electrodes for the sulfide detection in the aqueous media. Debora and his co-workers have been examined the response of a pre-oxidized nickel electrode electrochemically with increasing additions of sulfide to produce a voltametric signal [27]. Bitziou et. al. have been innovated a novel electrochemical approach to detect H<sub>2</sub>S in aqueous media within a broad pH range (acid to alkali) using a hydrodynamic flow cell with a dual band electrode device [28]. Giovanelli and co-workers have been modified a nickel hydroxide electrode at micro-disc and macroelectrodes in the existence and absence of sulfide with a detection limit of 10 µm [29]. Due to their commendable properties, screen-printed electrodes (SPEs) have introduced a new dimension to the electro analysis sector. The SPE technology has been developed as an interesting alternative cheap, highly sensitive and reusable sensors manufacturing [30,31]. The SPEs also surpass the additional mechanical polishing step that is routinely used to eliminate the adsorbed species in the case of solid electrodes, preventing any electrode fouling. In addition, the added value of using SPEs for direct sulfide oxidation is that sensing can be accomplished without the mediator or alteration of redox active polymers or metal composites being used [32-38].

The central theme of this work was directed to use a novel and innovate approaches for the early sensing of sulfate-reducing bacteria (SRB) in their planktonic form via estimation of their metabolites in the form of H<sub>2</sub>S gas with correlation to their numbers (ml). This can be achieved by develop an innovative electronic sensor via nano metal oxides-conductive polymer nanocomposites. The prepared materials were characterized using FT-IR, Raman spectroscopy, XRD, TEM, DLS and SEM. Furthermore, the prepared sensing materials were applied on the fabricated sensor with a customized design using a drop casting technique and tested towards biogenic H<sub>2</sub>S gas emitted from environmental SRB after cultivation and enumeration. The sensor response will be collected by a data acquisition system (digital multimeter) as an electrical change.

## 2. Experimental:

### 2.1. Chemicals

Cadmium nitrate (Cd(NO<sub>3</sub>)<sub>2</sub>·4H<sub>2</sub>O), Zinc Sulphate (ZnSO<sub>4</sub>), cerium (III) nitrate hexahydrate (Ce(NO<sub>3</sub>)<sub>2</sub>·6H<sub>2</sub>O), Polyethylene glycol-400 (PEG-

400), Sodium hydroxide (NaOH), Aniline monomer, Ammonia (NH<sub>4</sub>OH), Ammonium per sulphate (APS), Potassium per sulphate (KPS), Dodecyl benzene sulfonic acid (DBSA), All reagents were supplied from Sigma Aldrich. Hydrochloric acid (HCl), Butanol, Hexane, Acetone (AR grade) were supplied from Merk. Conducting Carbon Cement (Leit-C) was supplied from TAAB, UK.

### 2.2. Synthesis of polyaniline (PANI)

The first step was the oxidation in an aqueous medium. Aniline hydrochloride 0.2 M (2.59 g) was dissolved in a distilled water (DW) (50 ml) and 0.25 M (5.71 g) of APS was dissolved in a DW (50 ml). Both solutions were stored for 1 h at room temperature then mixed together, stirred and left to polymerize. After 24 h, the precipitate was filtered, washed with 300 ml of HCl (0.2 M) and acetone, then dried in a vacuum oven at 60 °C to obtain polyaniline (emeraldine) hydrochloride powder [39].

### 2.3. Synthesis of metal oxide nanoparticles

CdO NPs was prepared by dissolving 0.5 M (15.42 gm) of Cd(NO<sub>3</sub>)<sub>2</sub>·4H<sub>2</sub>O and 5 ml of ammonia solution in DW (100 ml) under stirring, then the gel suspension was filtrated and washed many times by DW, then dried at 50°C for 4 h. Finally, the dried powder was calcined at 600°C [40]. Also, ZnO NPs was prepared via mixing 0.5 M (2.17gm) of ZnSO<sub>4</sub> solution with 0.1 M (0.03gm) sodium hydroxide solution drop-wise and stirred for 1 h. Afterwards, the grain growth was prevented by adding few drops of PEG-400 as a capping agent. The solution was sonicated for 30 min, to obtain zinc hydroxide, then dried at 100°C for 8 h. then calcinated at 400°C for 2 h [41]. Finally, CeO<sub>2</sub> NPs was prepared via mixing 0.1 M (0.04 gm) of NaOH solution with 0.5 M (2.17 gm) of Ce(NO<sub>3</sub>)<sub>2</sub>·6H<sub>2</sub>O solution drop wise with continuous stirring at room temperature for 20 min, the mixture solution was centrifuged many times with DW and ethanol. The obtained precipitate was calcinated at 600° C for 20 min [42].

### 2.4. Synthesis of polymer nanocomposites (PANI/ZnO, PANI/CdO & PANI/CeO<sub>2</sub>)

2.5 g of KPS was dissolved in 60 ml of DW and added to a mixture of (40 ml of hexane, 6 ml of butanol, and 14 g of DBSA), the mixture sonicated for 5 min. Then a drop-wise addition of 2 ml of aniline

monomer to the prepared mini-emulsion was operated into a sono-chemical reactor followed by adding the metal oxide nanoparticles (5 wt% based on aniline monomer). The mixture was then ultrasonicated for 100 min until the polymerization completed. The reaction mixture was filtered, washed by acetone and water many times then dried by a vacuum at 40 °C for 24 h. [43].

## 2.5. Sensor fabrication

### 3.5.1. Electrical circuit and sensor design

The layout of the fabricated sensor and the circuit design were drawn by a computer numerical control machine (CNC) is a 4-axis control with built-in motion control CPU using Mach3 software. The designed electrode, separated by 1 mm. from its all sides, was fabricated on a printed circuit board (PCB) using CNC. The deposited films were prepared by mixing the carbon paste with the prepared materials by 10% (w/w) then spread over onto the fabricated electrode using drop casting technique uniformly. Afterwards, they allowed to dry under vacuum at room temperature for 24 h followed by Ag/AgCl ink print. Finally, insulating ink was applied.

### 3.5.2. Setup of the gas sensing unit

The lab tests were operated using a conical sealed glass chamber of 50 ml with gas inlet and outlet ports; the fabricated sensor was fitted inside the chamber firmly with its proper electrical connections. The H<sub>2</sub>S gas was injected through the chamber using gas flow meter at room temperature. The sensor electrical resistance changes were recorded using the attached computer supported 6-digit (Keithley 6514) System Electrometer which connected to the computer via GBIP interface). The reaction was a result of the sensing materials with H<sub>2</sub>S gas, at a constant voltage 0.1 V DC provided from an external electrical power supply. The H<sub>2</sub>S gas concentrations which were used in lab tests were obtained in 1-liter tedlar bag capacity then it was connected to the chamber. The sensor was placed in the chamber then H<sub>2</sub>S gas flow started to fill the chamber until complete occupation. During the test time the electrometer recorded, the resistance changed until reach the constant change then the chamber was allowed to air exposure before the second cycle of H<sub>2</sub>S exposure [44]. The experimental setup was illustrated in (Fig. 1) The gas response or gas sensitivity (S) was calculated as follows:

$$S \% = \frac{R_g - R_a}{R_g} \times 100 \dots \dots \dots (1)$$

where, R<sub>a</sub> is the initial resistance, R<sub>g</sub> is the resistance in the presence of the H<sub>2</sub>S gas.

To study the gas effect on the sensor response, the resistance was measured in the air and in the flow of H<sub>2</sub>S gas at the ambient temperature. The semi-prototype test chamber was designed and fabricated using the 3d printer (CREALITY 3D CR-10s 300MM).

## 2.6. Reactor setup and Sampling enrichment

A water sample with a salinity content (NaCl) of 1.9 % was gathered from the storage tank of North Bahria, Qarun Petroleum Company, western desert, Egypt. On site inoculation of the gathered water samples was achieved in an anaerobic culture media (modified Postgate's-B medium) referring to Postgate [45]. During preparation process the Postgate's medium was Modified using the original water salinity (NaCl) and pH (see Table 1). The prepared medium was sparged with nitrogen gas, and a redox potential indicator resazurin (0.0002 % w/v) for anaerobic cultivation has been used. The inoculated medium with 10 % (v/v) water samples was incubated at 37 °C for 14 days. The medium preparation and cultivation were accomplished referring to the modified Hungate's approach for anaerobes [46]. The presence of black precipitate (FeS) was used as a sulfate reduction sign and as a marker of SRB activity. For further cultivation, the inoculated sample was enriched using modified Postgate's-B medium for three times under anaerobic conditions to be used as inocula. In order to evaluate the sulfide production using the SPE, the SRB environmental sample was further inoculated with the enriched inocula and cultivated at 37 °C for 30 days using modified Postgate's-C medium according to Postgate [45]. The SRB count was estimated during the cultivation time using most probable number (MPN) [47].

## 2.7. Characterization techniques

The crystallography of nanoparticles was confirmed using X-ray Diffraction (XRD) using model (X'Pert Pro) 2 range from 5°-90° conditions 40 mA, 40 kV, and wave length of Copper Kα1 at 1.54 Å, with a Cu-Kα radiation (λ = 1.5406 Å) Diffractometer. The particle size and the morphology of the prepared nanoparticles were characterized using the High-Resolution Transmission Electron Microscopy (HR-TEM, JEOL JEM-2100F, Japan, 200 KV). The

particle size distribution was obtained using the Dynamic Light Scattering (DLS) with a laser angle of 90° at 25°C, (Zetasizer Nano-ZS90 instrument, Malvern Co., UK). The chemical structure and function groups of the prepared Polypyrrole were characterized by a Nicolet iS10 FT-IR spectrophotometer (Thermo Fisher Scientific, USA) in a wavenumber range of 500-4000 cm<sup>-1</sup>. The PANI molecular weight was recorded using Gel Permeation Chromatography (GPC), a GPC-water 2410 with a reflective index detector using 4 columns styragel HR THF 7.8 × 300 mm, calibrated by PS standard, supported a water 515 HPLC pump. Computer numerical control machine (CNC) SIM-KIT 40\*60 C-S, Simplex, Egypt. 3D Printer (CREALITY 3D CR-10s 300MM), China. The electrical measurements and the responses of the gas sensors were monitored using (Keithley instrument, Inc. USA) a Keithley source measurement unit (6514). The electrometer was interfaced to the computer via GPIB interface.

### 3. Characterization of prepared compounds

The FT-IR spectrum (Fig. 2) of the prepared polyaniline showed the main characteristic peaks of the base form of PANI ranged 1600-500 cm<sup>-1</sup>. The main bands located at 1559 cm<sup>-1</sup> for C-H bond vibration, 1481 cm<sup>-1</sup> for C=C bond vibration, and 1370 cm<sup>-1</sup> assigned to C-N bond vibration. The Raman spectrum of the prepared PANI (Fig. S1) displayed a peak of the C=C stretching vibration at 1602 cm<sup>-1</sup> with a shoulder at 1636 cm<sup>-1</sup>. The C-C vibration contribute to the band at 1571 cm<sup>-1</sup>. The band at 1476 cm<sup>-1</sup> was corresponded to the C=N stretching vibrations. A sharp band at 1378 cm<sup>-1</sup> and 1414 cm<sup>-1</sup> were assigned to the C~N+ ring stretching vibrations. A shoulder observed at 1352 cm<sup>-1</sup> was related to the C~N+. The molecular weight of the prepared PANI Mw= 15080 g/mol and the polydispersity PDI= 3.6. The SEM image of the prepared PANI (Fig. 3) exhibited the bulky structure of PANI with micro-porous structures which improved the performance of the polymer conductivity properties and rising up the sensing rate as a result of the large surface area consistence [44].

Along the same line, the morphological properties and the particle size distributions of the prepared materials were determined by HR-TEM Fig. 4 (a-c) and DLS Fig. S2 (a-c). The data from Fig. 4a determined the nanocrystalline particles with a weak agglomeration of hexagonal ZnO NPs and particle size

20 nm. While Fig. 4b observed a uniform cubic structure of CdO NPs and particle size 23 nm. Furthermore, Fig. 4c confirmed the spherical shape of CeO<sub>2</sub> NPs and particle size 37 nm, according to Fig. S2 (a-c) the zeta potential and PDI values confirms the homogeneity of the prepared metal oxides with high crystallinity. Also, The XRD patterns of the prepared materials were shown in Fig. 5 (a-c) and the particles

$$D = \frac{0.9\lambda}{\beta \cos \theta} \dots\dots\dots(2)$$

average size were calculated by Debye-Scherrer's equation as follows.

Where D is the crystal size, λ is the x-ray wavelength, β is the full width at half maximum of the diffraction peak, θ is the Bragg diffraction angel.

The data observed from Fig. 5a, all the peaks of (1 0 0), (0 0 2), (1 0 1), (1 0 2), (1 1 0), (1 0 3), (2 0 0), (1 1 2), (2 0 1), (0 0 4) and (2 0 2) values can be referred to the hexagonal structure of ZnO NPs. These peaks match with those in the JCPDS card (Card No. 89-1397). The high intensity and narrow width of ZnO diffraction peaks confirmed that the resulting product has a high crystallinity with calculated average size about 20.95 nm.

The crystalline centered cubic symmetry structure of CdO, (see Fig. 5b) with the plane of (111), (200), (220) was matched with the JCPDS card (Card No. 65-2908). and the calculate particle size is about 22.87 nm. It can be concluded from Fig. 5c that all the diffraction peaks of the CeO<sub>2</sub> can be assigned to JCPDS card (Card No. 89-8436). The characteristic two peaks of 28.51, 47.51 and 56.58 were corresponded to the reflection planes of (111), (220) and (311), respectively. The sharp and intense diffraction peak indicated the crystallinity. The calculated average size of CeO<sub>2</sub> is about 36.35 nm.

Finally, the HR-TEM images of the prepared polymer nanocomposites were shown in Fig. 6(a-c). The ZnO NPs (see Fig. 6a) have been well entrapped in the PANI matrix with a micro structured morphology. While Fig. 6b Referring to the PANI/CdO, observed that a homogeneous distribution of CdO NP onto the PANI matrix with a spherical structure. It can be observed that from Fig.6c the porous structure morphology of PANI/CeO<sub>2</sub> nanocomposite was different from the individual spherical CeO<sub>2</sub> NP as the first stage of the metal oxide preparation. Its meaning that, the in-situ polymerization has been produced nanocomposites without agglomeration and the prepared metal NPs were distributed uniformly in the polymer matrix to enhancement the conductivity of the prepared materials [43].

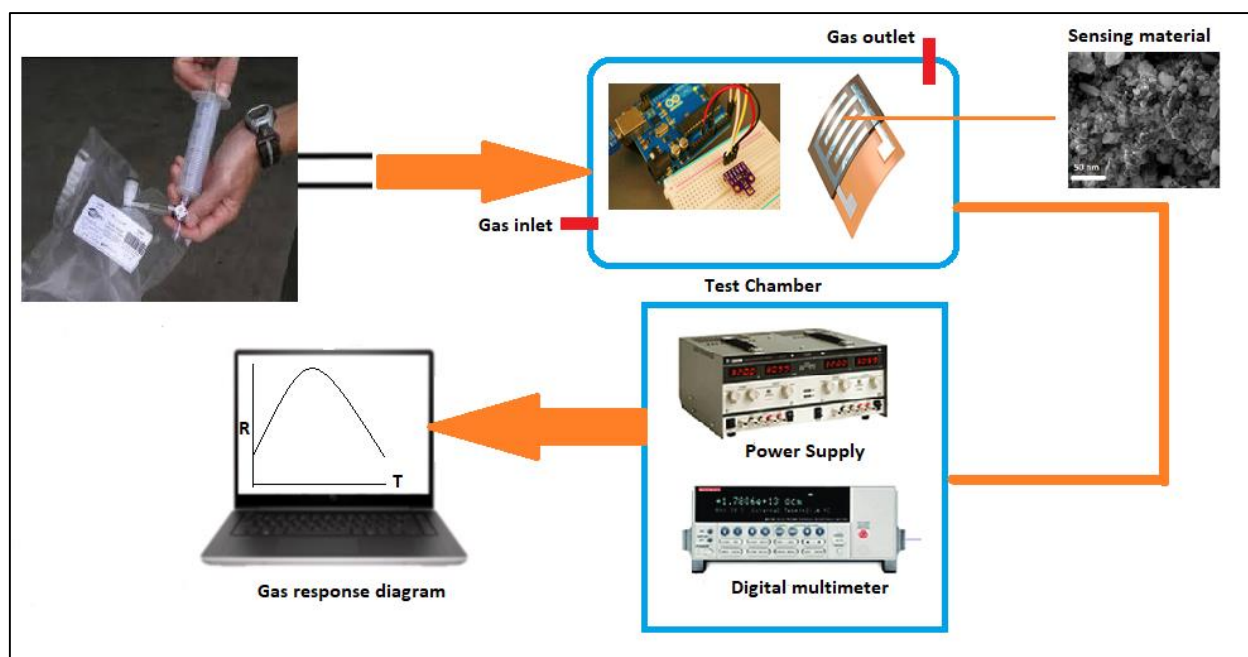


Fig.1

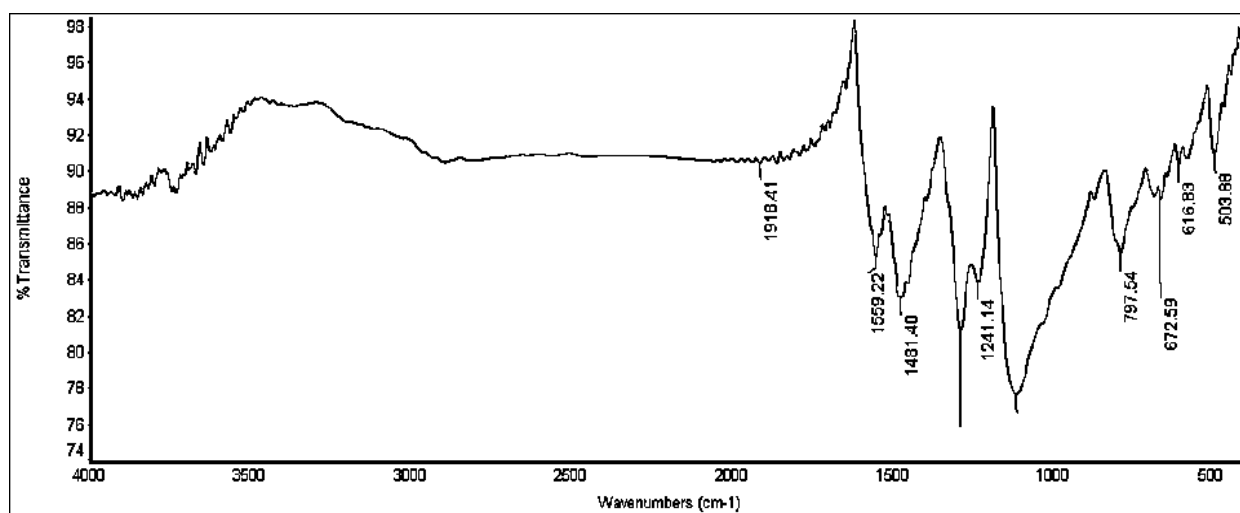


Fig.2

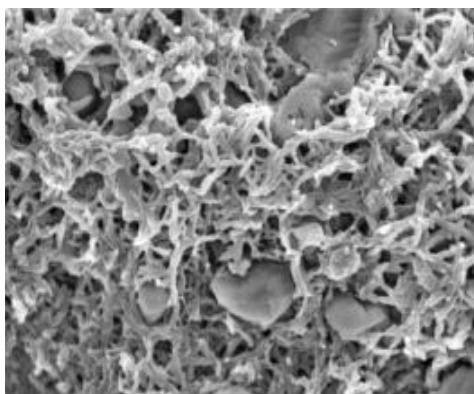


Fig. 3

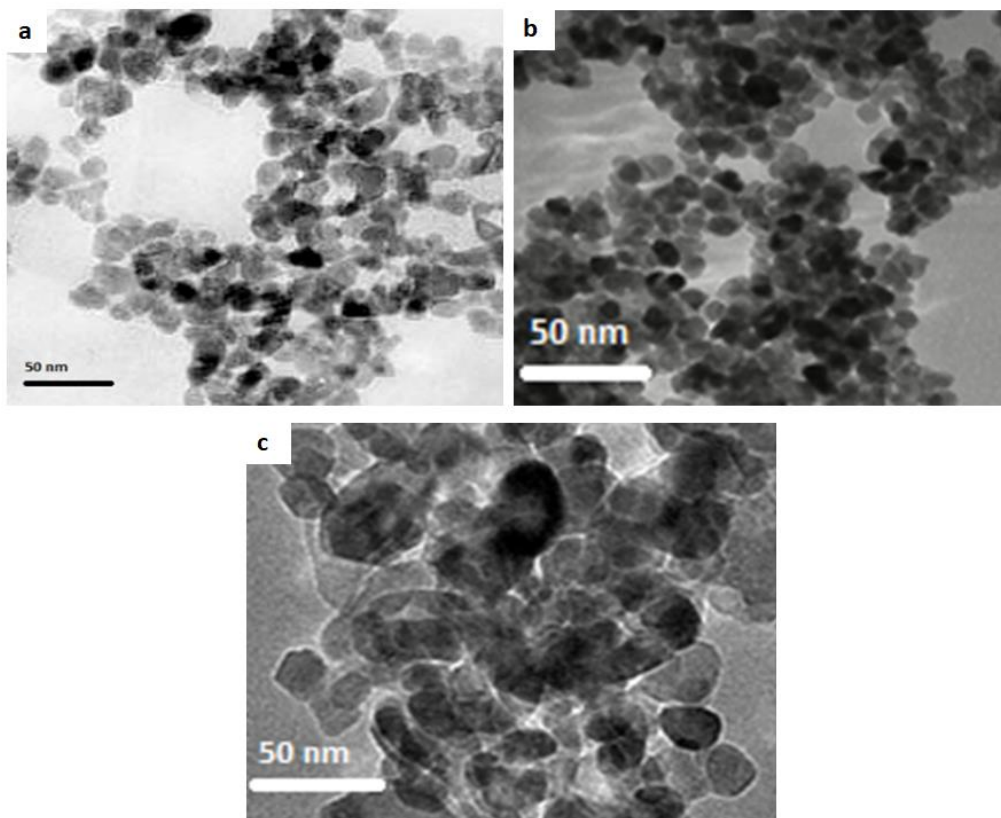


Fig. 4

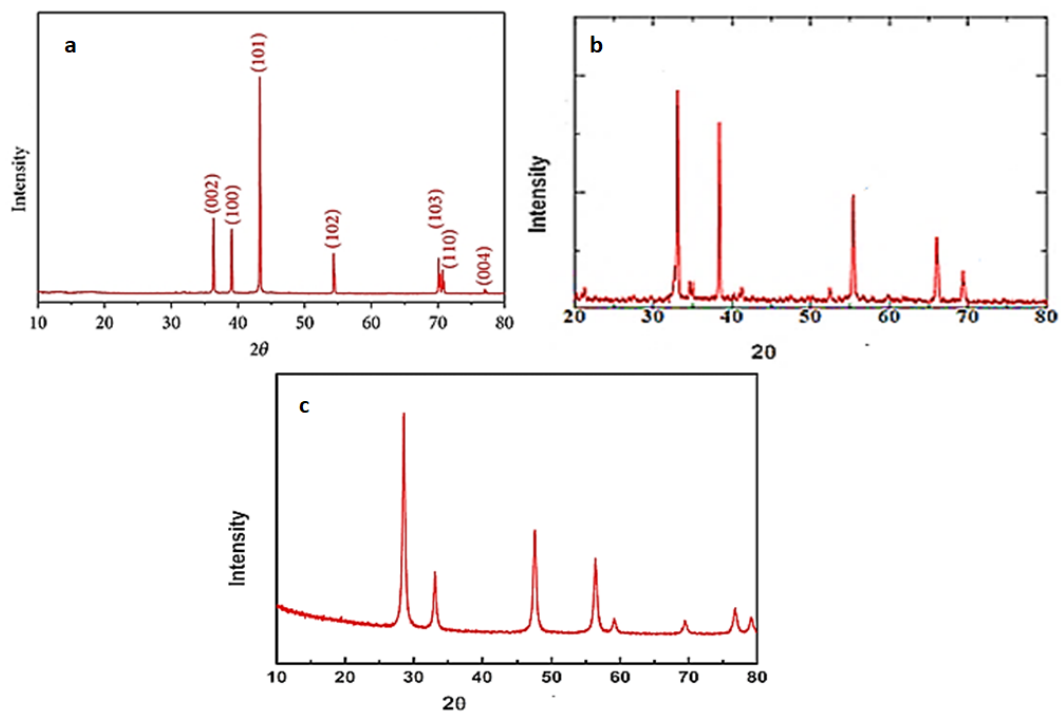


Fig. 5

Table 1: Composition of anaerobic\* modified *Postgate's B* (P<sub>B</sub>) medium

Composition (g/l)	Modified P <sub>B</sub>	Modified P <sub>C</sub>
KH <sub>2</sub> PO <sub>4</sub>	0.5	0.5
NH <sub>4</sub> Cl	1.0	1.0
Na <sub>2</sub> SO <sub>4</sub>	1.0	4.5
CaCl <sub>2</sub> .6H <sub>2</sub> O	-	0.06
MgSO <sub>4</sub> .7H <sub>2</sub> O	2.0	0.06
Sodium lactate	3.5	4.42
Yeast extract	1.0	1.0
Ascorbic acid	0.1	-
Sodium thioglycolate	0.1	-
FeSO <sub>4</sub> .7H <sub>2</sub> O	0.5	-
Sodium citrate. 2H <sub>2</sub> O	-	0.3
Salinity (NaCl)	19	19
pH	6.76	6.76

\*0.0002% (w/v) resazurin was used as a redox potential indicator for anaerobic cultivation.

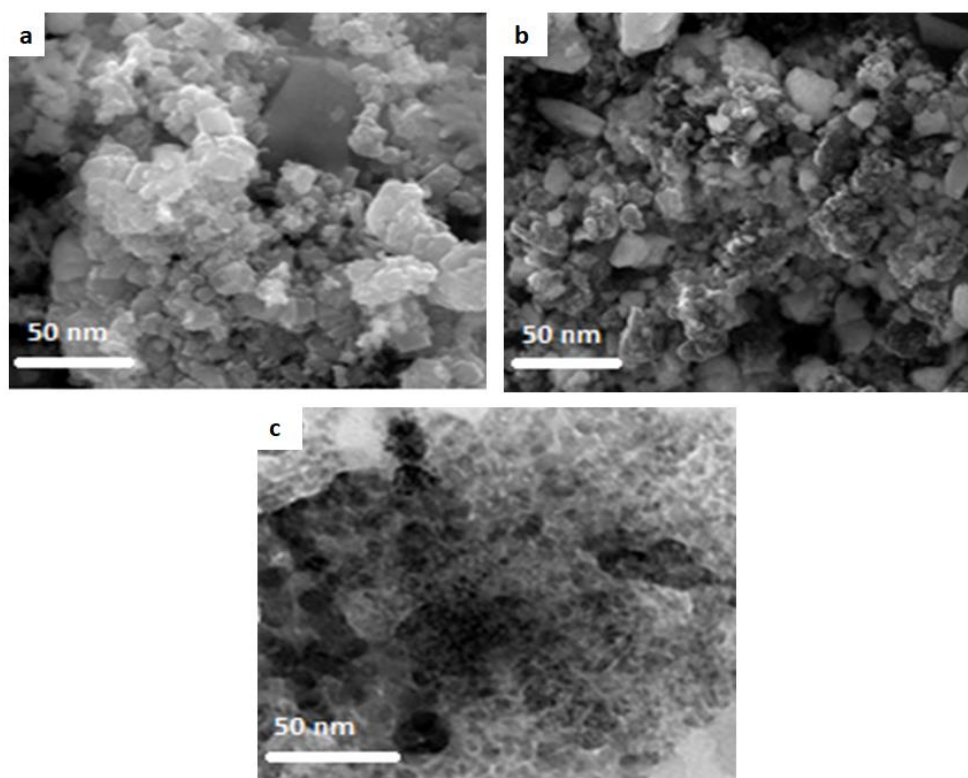


Fig. 6

#### 4. Results and Discussion

##### Gas sensing properties of PANI and PANI/MOx Nanocomposites.

The response of the fabricated sensors was calculated according to eq.1 The exposure of sensors to H<sub>2</sub>S gas, an electron donor, is leading to increase the resistivity and decrease the conductivity. Therefore, the response *S* (%) has always a positive sign. Thus, the increase in the resistance of the PANI/MOx nanocomposites after the exposure to H<sub>2</sub>S gas was established with the increase in the resistance of the PANI that formed by reducing in the electron hopping.

It is well recognized that nano-metal oxide dopants will enhance the sensing efficiency of polymer-based gas sensors [17]. The sensing properties of the PANI and PANI/MOx nanocomposite thin films towards the biogenic H<sub>2</sub>S gas were measured firstly using Dräger tube test. This test was used to determine the real gas concentrations [48] with a correlation to the most probable number of the cultivated sulfate-reducing bacteria (SRB) [47]. Afterwards, the PANI and PANI/MOx nanocomposite was applied as a fabricated sensor to detect the changes in the electrical response. Results reported in Table 2 and Fig. 7 confirmed the sensing ability of the prepared materials towards the released biogenic H<sub>2</sub>S gas with concentrations (100, 1000, 2000 and 3000 ppm) after cultivation periods (5, 10, 20 and 30 days) were named (D5, D10, D20 and D30) respectively. The cultivated plank samples have been measured by a widely used detector tube standard in the petroleum sector Dräger-Tubes and Dräger-Tube pump accuro, which are tested referring to NIOSH Method/TCA/A-012 and approved by the American Industrial Hygiene Association (AIHA).

Thus, it can be observed that the highly sensitive sensor with short response time at all H<sub>2</sub>S gas concentrations is the sensor layered by PANI/ZnO NPs, the data displayed that there was an increase in the sulfide gas concentration accordingly with increase in the most probable number of the cultivated samples during the cultivation period (30 days) (see Fig. S3). This defiantly correlated to the SRB activity as previously reported [47]. The sensitivity of the prepared materials PANI, PANI/MOx nanocomposites at room temperature and H<sub>2</sub>S concentration 1000 ppm (sample D10) have been illustrated as 3 cycles at Fig. S4. The data showed that

the polymer nanocomposite films were charge carriers which known as p-type semiconductors with holes. The H<sub>2</sub>S gas is dissociated into H<sup>+</sup> and HS<sup>-</sup> according to its behavior as a weak acid, leading to the partial protonation of PANI. A band bending and a space-charge layer near the surface of each grain boundary were therefore induced. [43]. The electrical resistance of the film changes as a result of the interactions between the surface grains and the introduced H<sub>2</sub>S gas moieties, causes electrons elimination of the PANI aromatic ring. So, the resistance of the sensing materials affected by these electron transfer. When this reaction of the p-type conductive polymer occurs, its electrical conductivity may enhance [44]. Moreover, the observed data going to prove the highly sensitive sensor is the sensor layered by PANI/ZnO NPs with the shorter response time. It is clear that from the real-time of the sensing responses towards the variable concentrations of H<sub>2</sub>S gas at room temperature was increased rapidly by exposing to the H<sub>2</sub>S gas and returned to its initial value after air introduction.

As a result, it can be seen that the prepared nano composites have high sensitivity with short response times comparing to the pure polymer, proving that the introducing of metal oxides into the polymer matrix improve its conductivity properties [49]. This result confirmed that the sensors responded quickly to both the induction and removal of the H<sub>2</sub>S gas. Through the three cycles of testing process using the same sensors, the sensor response (%) decreased and the response time increased. In brief, the data showed that the response time of PANI/ZnO < PANI/CdO < PANI/CeO<sub>2</sub> < PANI, Meanwhile, the sensitivity showed PANI/ZnO > PANI/CdO > PANI/CeO<sub>2</sub> > PANI which confirmed that the PANI/ZnO has the fastest response time with high sensitivity. Its may be attributed to the microstructure, high porosity, high surface area with small average size about 20 nm. enhancement the properties of ZnO NPs nanocomposite and increasing the oxygen vacancies with decreasing the surface potential barriers. As the same for the PANI/CdO NPs the difference only the particle size of CdO NPs is a little bigger than ZnO NPs about 23 nm. leading to a little increase on the its surface area which will affect on its sensitivity. On the other hand, PANI/CeO<sub>2</sub> has the lowest sensitive material than the others affected by the changes on its morphology when introduced to the polymer matrix, also its average particle size is bigger than the others

leading to increase its surface area and decreasing its sensitivity. Although, PANI/CeO<sub>2</sub> is the lowest sensitive material but it has a higher response to the biogenic H<sub>2</sub>S gas than the PANI only.

The repeatability of the sensing process had been studied by repeating the test of the fabricated sensors towards the biogenic H<sub>2</sub>S gas (1000 ppm) at room temperature. It is worthwhile to mention that from Fig. 8, the recorded values for the sensor's responses with respect to time. the results of each sensor possess a

variation of  $\pm 0.01\%$ . The fabricated sensors demonstrated a good stability toward H<sub>2</sub>S gas at room temperature, which confirmed a stable morphology and good crystallinity of the fabricated sensing materials. Furthermore, the above data confirmed that the performance of the PANI/ZnO nanocomposite possess the highest sensitivity and the fastest response time affected by its morphological properties and the highly surface area with the smallest particle size compared to the other materials.

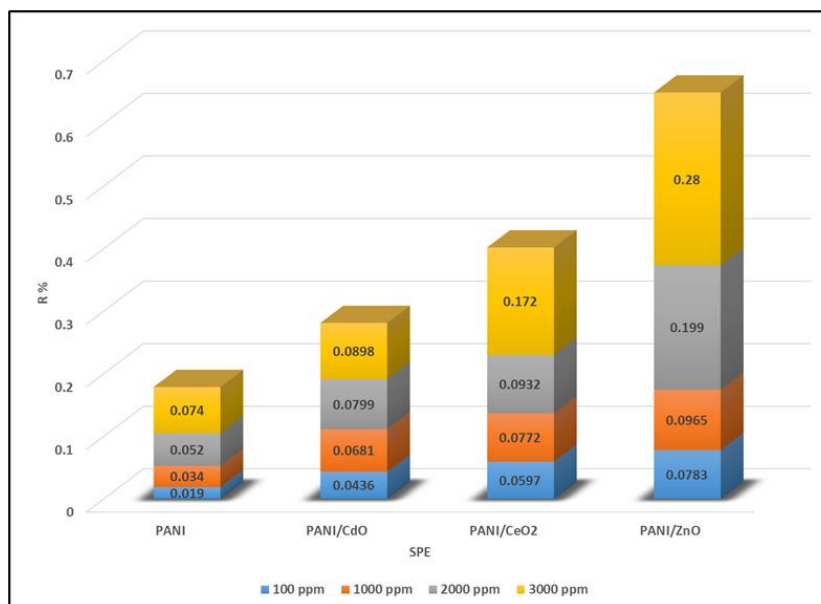


Fig. 7

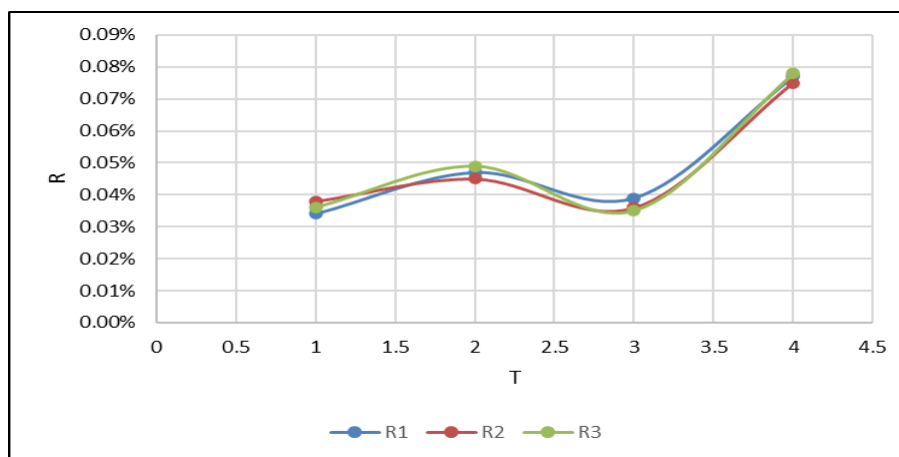


Fig. 8

Table 2: The response of the fabricated sensors towards H<sub>2</sub>S gas at room temperature

Sample no.	H <sub>2</sub> S reading by Dräger tube, ppm	H <sub>2</sub> S gas response, %			
		PANI	PANI/CdO	PANI/CeO <sub>2</sub>	PANI/ZnO
D5	100	0.019	0.0436	0.0597	0.0783
D10	1000	0.034	0.0681	0.0772	0.0965
D20	2000	0.052	0.0799	0.0932	0.199
D30	3000	0.074	0.0898	0.172	0.276

Table 3: The 3 cycles response tests of the fabricated sensors towards 1000 ppm of H<sub>2</sub>S gas at room temperature

Sample	Cycle 1		Cycle 2		Cycle 3	
	R, %	T, s	R, %	T, s	R, %	T, s
PANI	0.034	60	0.028	75	0.01	140
PANI/CdO	0.047	26	0.027	43	0.022	60
PANI/CeO <sub>2</sub>	0.039	37	0.021	68	0.013	85
PANI/ZnO	0.077	10	0.056	22	0.038	54

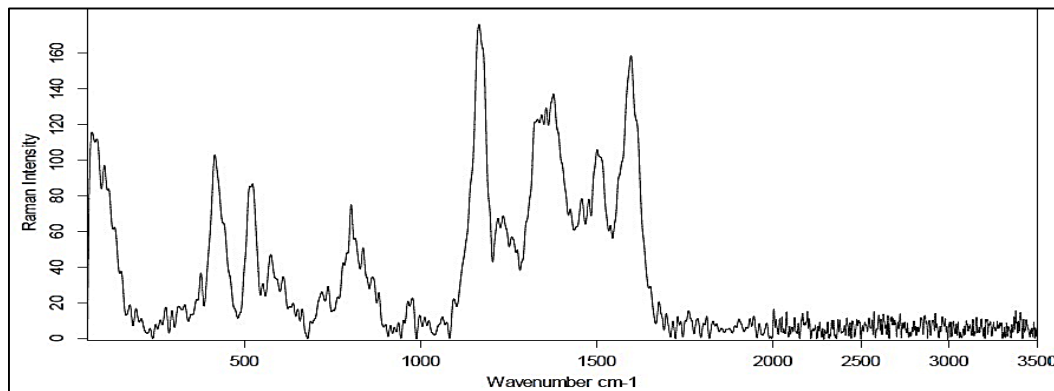
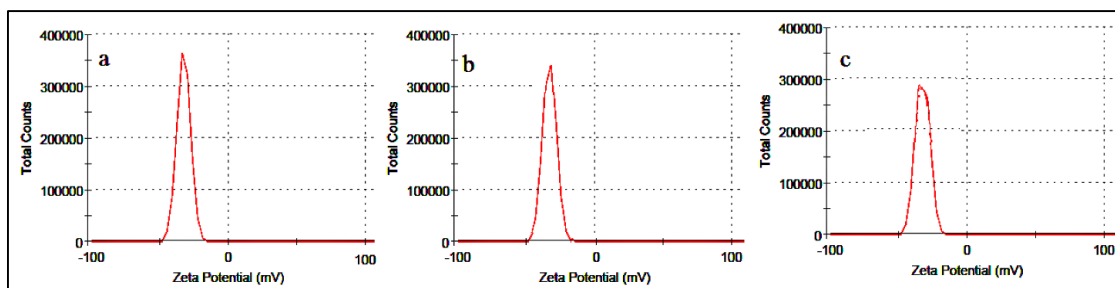
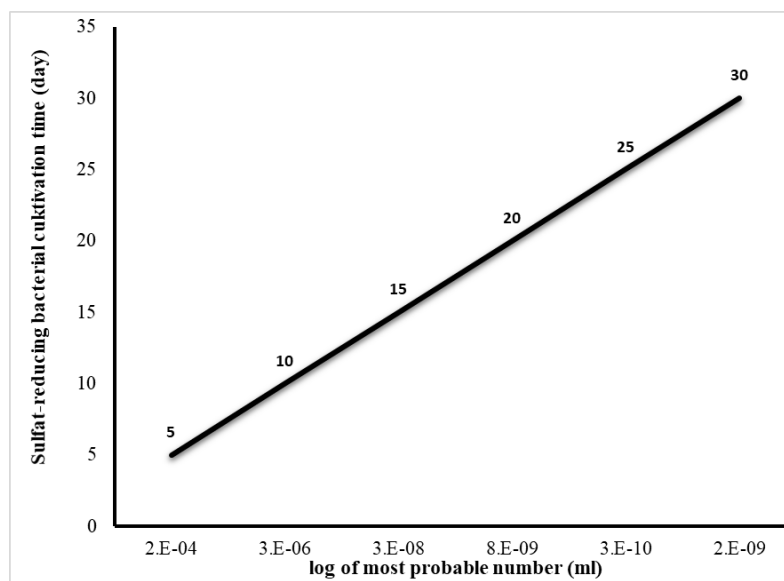


Fig. S1: Raman spectrum of PANI

Fig. S2: The DLS Zeta potential distribution of: a) ZnO, b) CdO, c) CeO<sub>2</sub>Fig. S3: The correlation between H<sub>2</sub>S gas concentrations and MPN of cultivated samples

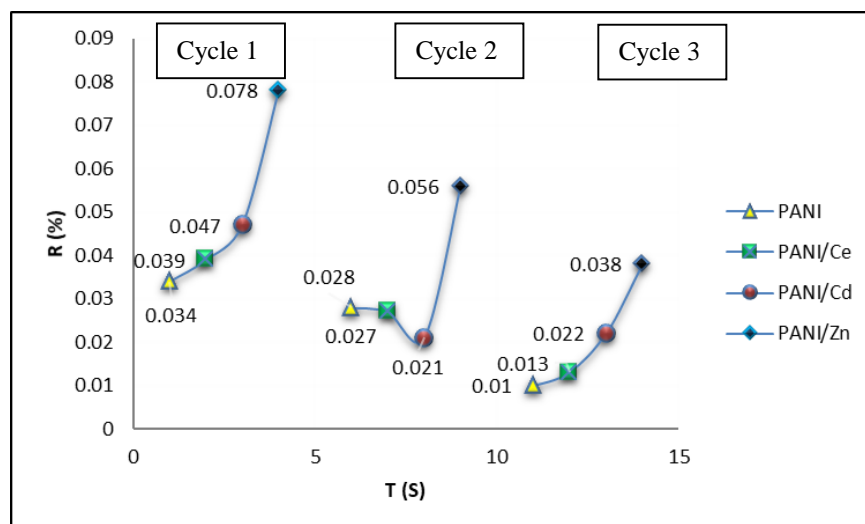


Fig. S4: The sensitivity and reusability of fabricated sensors through 3 cycles of testing process

## 5. Conclusions

The sensing materials PANI, PANI/ZnO NPs, PANI/CdO NPs and PANI/CeO<sub>2</sub> NPS were successfully prepared and characterized using several techniques, and applied on newly designated PCB circuit using a drop casting technique to fabricate novel sensors for the fast detection of the biogenic H<sub>2</sub>S gas, which considered as a good marker of the SRB existence. The microstructure, high surface area, high porous sites are the main factors affect on the prepared materials behavior. As well as, affected on the response of the fabricated sensors towards the biogenic H<sub>2</sub>S gas at different concentrations (100, 1000, 2000 and 3000 ppm). It's clear that the response time of PANI/ZnO < PANI/CdO < PANI/CeO<sub>2</sub> < PANI and the sensitivity of PANI/ZnO > PANI/CdO > PANI/CeO<sub>2</sub> > PANI. The lower response is PANI (R= 0.034 %) with highly response time (60 s), the higher response is PANI/ZnO NPs (R= 0.077%) with fastest response time (10 s). its may be referred to the crystallinity, high porosity and high selectivity of ZnO NPs which increased the oxygen vacancies sites leading to increase of oxygen species adsorption, hence decreasing the potential barriers of the prepared material surface and improve the workability of conducting polymer. In addition, the smallest particle size of ZnO (20 nm) play an important role to enlarge the surface area leading to increasing the exposure area towards the biogenic H<sub>2</sub>S gas which reflect on its highly response comparing to the other hybrid nanocomposites.

## 6. Conflicts of interest

“There are no conflicts to declare”.

## 7. Formatting of funding sources

The Academy of Scientific Research and Technology (ASRT), JESOR call - project number (28).

## 8. Acknowledgments

The authors are grateful to the Academy of Scientific Research and Technology (ASRT), JESOR call - project number (28). Egyptian Petroleum Research Institute (EPRI), Cairo, Egypt.

## References

- [1] Abdolahi A, Hamzah E, Ibrahim Z, Hashim S, Corros Rev, 2014, 32, 129–141.
- [2] Kushkevych I, Kollar P, Ferreira A.L, Palma D, Duarte A, Lopes M.M, Bartos M, Pauk K, Imramovsky A, Jampilek J, J. Appl. Biomed., 2016, 14, 125–130.
- [3] Foti M, Sorokin DY, Lomans B, Mussman M, Zacharova EE, Pimenov NV, Kuenen GJ, Muyzer G. Appl Environ Microbiol. 2007, 73, 2093–2100.
- [4] Folwell BD, McGenity TJ, Price A, Johnson RJ, Whitby C, Int Biodeter Biodegr, 2015, 108, 214–22.
- [5] Shi, X, Yan W, Xu D, Yan M, Yang C, Shan Y, Yang K, J. Mater. Sci. Technol, 2018, 34, 2480–2491.
- [6] Usher K.M, Kaksonen A.H, Cole I, Marney D, Int. Biodeterior. Biodegrad, 2014, 93, 84–106.
- [7] Jia R, Unsal T, Xub D, Lekbach Y, Gu T, Int. Biodeterior. Biodegrad, 2019, 137, 42–58.
- [8] Liu, H.; Sharma, M.; Wang, J.; Cheng, Y.F.; Liu, H. Microbiologically influenced corrosion of 316L stainless steel in the presence of *Chlorella vulgaris*. Int. Biodeterior. Biodegrad. 2018, 129, 209–216.

- [9] Liu H, Cheng Y.F, *Electrochim. Acta*, 2018, 266, 312–325.
- [10] Queiroz G.A.D, Andrade H.S, Malta T.B.S, Vinhas G, Lima M.A.G.D.A, *Mater. Res*, 2018, 21, e20170338.
- [11] Fossing H, Jørgensen B. B, *Biogeochemistry*, 1989, 8, 205–222.
- [12] Gibson G.R, Parkers R.J, Herbert R.A, *J Microbiol Methods*, 1987, 7, 201–210.
- [13] Flemming V, Kjeld I, *Appl Environ Microbiol*, 1998, 64(5), 1700–1707.
- [14] Ruas de Souza A, Foster C, Kolliopoulos A, Bertotti M, Banks C, *Analyst*, 2015, 140, 4130–4136.
- [15] Smith J, Metters J, Irving C, Sutcliffe O, Banks C, *Analyst*, 2014, 139, 389–400.
- [16] Bernalte E, Marín Sánchez C, Pinilla Gil E, *Electroanalysis*, 2013, 25, 289–294.
- [17] Pandey S, Kim K, Tang K, *Trends Anal. Chem*, 2012, 32, 87–99.
- [18] Radford-Knoery J, Cutter G, *Anal. Chem*, 1993, 65, 976–982.
- [19] Bailey T, Pluth M, *J. Am. Chem. Soc*, 2013, 135, 16697–16704.
- [20] Colon M, Iglesias M, Hidalgo M, Todoli J, *J. Anal. At. Spectrom*, 2008, 23, 416–418.
- [21] Lawrence N, Davis J, Compton R, *Talanta*, 2000, 52, 771–784.
- [22] Asad M, Sheikhi M, Pourfath M, Moradi M, *Sens. Actuators, B*, 2015, 210, 1–8.
- [23] Berahman M, Sheikhi M, *Sens. Actuators, B*, 2015, 219, 338–345.
- [24] Fam D, Tok A, Palaniappan A, Noppawan P, Lohani A, Mhaisalkar S, *Sens. Actuators, B*, 2009, 138, 189–192.
- [25] Zhao M, Wang X, Ning L, Jia J, Li X, Cao L, *Sens. Actuators, B*, 2011, 156, 588–592.
- [26] Schiavon G, Zotti G, Toniolo R, Bontempelli G, *Anal. Chem.*, 1995, 67, 318–323.
- [27] Giovanelli D, Lawrence N, Jiang L, Jones T, Compton R, *Analyst*, 2003, 128, 173–177.
- [28] Bitziou E, Joseph M, Read T, Palmer N, Mollart T, Newton M, Macpherson J, *Anal. Chem.*, 2014, 86, 10834–10840.
- [29] Giovanelli D, Lawrence N, Jiang L, Jones T, Compton R, *Sens. Actuators, B*, 2003, 88, 320–328.
- [30] Metters J, Kadara R, Banks C, *Analyst*, 2011, 136, 1067–1076.
- [31] Metters J, Kampouris D, Banks C, *Analyst*, 2014, 139, 3999–4004.
- [32] Wang T, Randviir E, Banks C, *Analyst*, 2014, 139, 2000–2003.
- [33] Ramdani O, Metters J, Figueiredo-Filho L, Fatibello-Filho O, Banks C, *Analyst*, 2013, 138, 1053–1059.
- [34] Wang J, Tian B, Nascimento V, Angnes L, *Electrochim. Acta*, 1998, 43, 3459–3465.
- [35] Laschi S, Fránek M, Mascini M, *Electroanalysis*, 2000, 12, 1293–1298.
- [36] Falciola L, Pifferi V, Mascheroni E, *Electroanalysis*, 2012, 24, 767–775.
- [37] Smith J, Metters J, Kampouris D, Lledo-Fernandez C, Sutcliffe O, Banks C, *Analyst*, 2013, 138, 6185–6191.
- [38] Slater J, Dilleen J, *Electroanalysis*, 1997, 9, 1353–1359.
- [39] Ahmed A. Farag, Khalid I. Kabel, Elsayed M. Elnaggar, Abdalrhman G. Al-Gamal, *Corros Rev*, 2017, 35(2), 85–94.
- [40] Thema F, Beukes P, Gurib-Fakim A, Maaza M, *J. of Alloy and Compd*, 2015, 646, 1043–1048.
- [41] Yadav B, Srivastava R, Yadav A, Srivastava V, *Sensor Letters*, 2008, 714, 1–5.
- [42] Jang Y, Kim K, Tsay O, Atwood D, Churchill D, *Chem. Rev.*, 2015, 115, 1–76.
- [43] Zhu C, Chou S, He S, Liao W, Chen C, *Nanotechnology*, 2007, 18(27), Article ID 275604.
- [44] Al-Sabagh A, Kabel K, Zaki T, Badawi A, Abdel Rahman A, Gado W, *Egypt. J. Chem.*, 2020, 63, 2763 - 2774.
- [45] Postgate J, Cambridge University Press, London and New York, 1984, 30–100.
- [46] Miller T, Wolin M, *Appl Microbiol*. 1974, 27, 985–987
- [47] Zietek B, Banasiewicz A, Zimroz R, Szrek J, Gola S, *Energies*, 2020, 13, 6331.
- [48] Sun X et al., *PDA J Pharm Sci Tech*, 2006, 60(2), 124–134.
- [49] Yan Y, Yang G, Xu J, Zhang M, Kuo Ch, Wang S, *Science and Technology of Advanced Materials*, 2020, 21,1, 768–786.